Article

Aqueous Potassium Salt of L-Cysteine as Potential CO$_2$ Removal Solvent: An Investigation on Physicochemical Properties and CO$_2$ Loading Capacity

Tengku Nur Adibah Tengku Hassan [1] , **Azmi Mohd Shariff** [1,*] , **Nor Faiqa Abd Aziz** [1] ,
Nur Farhana Ajua Mustafa [1] , **Lian See Tan** [2] , **Hairul Nazirah Abdul Halim** [3] , **Mustakimah Mohamed** [1]
and Heri Hermansyah [4]

[1]   CO2 Research Centre (CO2RES), Institute of Contaminant Management (ICM),
      Universiti Teknologi PETRONAS, Seri Iskandar 32610, Malaysia; tengku_19000950@utp.edu.my (T.N.A.T.H.);
      faiqa.aziz@utp.edu.my (N.F.A.A.); farhana.mustafa@utp.edu.my (N.F.A.M.);
      mustakimah.md@utp.edu.my (M.M.)
[2]   Department of Chemical Process Engineering, Malaysia-Japan International Institute of Technology,
      Universiti Teknologi Malaysia, Jalan Sultan Yahya Petra, Kuala Lumpur 54100, Malaysia; tan.liansee@utm.my
[3]   Faculty of Chemical Engineering & Technology, Universiti Malaysia Perlis, Kompleks Pusat Pengajian Jejawi,
      Arau 302600, Malaysia; hairulnazirah@unimap.edu.my
[4]   Department of Chemical Engineering, Faculty of Engineering, Universitas Indonesia, Depok 16424, Indonesia;
      heri.hermansyah@ui.ac.id
*   Correspondence: azmish@utp.edu.my; Tel.: +60-53687530

Abstract: The operational and economic constraints suffered by amine solvents for CO$_2$ removal have motivated the research on an alternative solvent with better performance and cost-effectiveness. Amino acid salt (AAS) has been identified as an interesting green solvent, an alternative to commercial amine solvents. The present work evaluated the physicochemical and CO$_2$-solubility properties of potassium L-cysteine (K-CYS), a naturally occurring amino-acid-based solvent for CO$_2$ removal from natural gas. Its physicochemical properties, including density, viscosity, and refractive index, were measured at different temperatures ranging between 298.15 and 333.15 K and a concentration range of 5 to 30 wt.%. Based on the experiment, all properties were found to decrease with increasing temperature and increase with increasing concentration. The experiments also demonstrated a significant reduction of CO$_2$ loading from 2.4190 to 1.1802 mol of CO$_2$/mol of K-CYS with increasing solvent concentration from 10 to 30 wt% at 313.15 K and 20 bar (g).

1. Introduction

Global energy demand has continuously risen due to accelerated growth in the human population, economic development, and modernization of technology. In May 2022, the International Energy Agency (IEA) reported that the energy demand in Southeast Asian countries has significantly expanded at an average of 3% per year over the past two decades. The trend is expected to persist until 2030 [1]. Natural gas (NG), one of the fossil fuels that mainly comprises methane (CH$_4$), serves as one of the important energy commodities for power generation. According to the IEA [1], NG consumption in Southeast Asian countries soared by more than 80% between 2000 and 2020, whereby the electricity and industry sectors accounted for about 70% of natural gas use. On the other hand, the Wood MacKenzie Report forecasted that the liquid natural gas (LNG) demand in Peninsular Malaysia will reach 7.2 million metric tons per annum (mmtpa) by 2023 and 13 mmtpa by 2030 [2]. Hence, these scenarios drive the need to further explore and monetize the undeveloped gas fields to accommodate domestic demand and ensure a sustainable energy supply.

However, many discovered gas fields remain undeveloped due to the bulk CO_2 content that varies between 20% and 80%, especially in the offshore areas of Thailand and Malaysia [3]. Approximately 23 trillion cubic feet (tcf) of undeveloped natural gas reserves have been identified today in Malaysian waters [4]. Battersby [5] foresees that, by 2030, 50% of Sarawak's gas output and 15% of Peninsular Malaysia's production will be produced from high-CO_2 fields. Therefore, CO_2 removal is a crucial task to exploit and monetize low-quality gas fields. Nevertheless, the development of highly sour gas fields is restricted by a few technical challenges due to the bulk CO_2 content and high pressure in the gas reservoir up to 200 bar [6]. Thus far, various technologies have been adopted to sequester bulk CO_2 from natural gas, including absorption, adsorption, membrane, and cryogenic separation.

Chemical absorption has been widely used on an industrial scale for more than 50 years due to its practicality and feasibility for industrial applications [7–10]. Since the 1930s, primary and secondary alkanolamines have been widely used as the solvents of choice for CO_2 removal by chemical absorption [11–13]. However, the drawback of using alkanolamines for CO_2 removal is that the reaction of CO_2 with amines is highly exothermic [14]. As a result, extensive energy input up to 4.75 GJ/tonCO_2 is necessary for the regeneration step to reverse the reaction and strip off CO_2 from the rich amines [15–17]. Moreover, these carbamate-forming amines have a lower equilibrium capacity for CO_2 [18]. In addition, the utilization of amine solvents is subjected to a few constraints, such as high vapor loss, thermal degradation, very toxic, corrosive, and high energy consumption for regeneration [8,19–22]. In the past decades, monoethanolamine (MEA) dominated the industrial CO_2 absorption process due to its high reaction rates and low cost [23]. Nevertheless, the maximum CO_2 loading capacity of MEA is limited to 0.5 mol CO_2/mol amine due to the formation of stable carbamates during the reaction. Under some circumstances, such as high pressure, hydrolysis of the carbamates formed may occur and potentially increase the CO_2 loading of MEA beyond 0.5 mol CO_2/mol MEA [24]. To date, the interest in the utilization of tertiary amines such as N-methyldiethanolamine (MDEA) for CO_2 removal has significantly increased owing to their interesting features, such as low vapor pressure and heat of absorption, as well as high thermal stability. Based on stoichiometry, MDEA exhibits a high CO_2 equilibrium loading capacity of up to 1.0 mol of CO_2/mol amine [25]. Despite these advantages, the efficiency of MDEA is restricted by its slow reaction rate with CO_2, as well as low absorption capacity at low CO_2 content [26,27].

To date, various studies have been reported in the literature to improve the CO_2 absorption of MEA and MDEA through blended solvents. Research has indicated that the effectiveness of the solvent mixture for CO_2 extraction can be enhanced by combining MDEA with activators. 2-Amino-2-methyl-1-propanol (AMP), piperazine (PZ), amino ethyl ethanol amine (AEEA), and diethanol amine (DEA) are the common activators used to increase the reaction kinetics and absorption capacity of aqueous amine solvents [28,29]. In industry, PZ blended with MDEA has been commonly employed as the standard solvent for purifying natural gas. For instance, Yuan et al. [28] employed piperazine-activated MDEA to enhance CO_2 absorption. The study revealed that the presence of PZ in the blended solvent resulted in the acceleration of the CO_2 absorption rate by 131%. Meanwhile, MDEA activated with PZ demonstrated a substantial increase in CO_2 loading from 0.45 mol/kg to 0.79 mol/kg compared to aqueous MDEA. However, its environmental impact is still suboptimal despite its impressive performance [30]. Hence, efforts are being directed towards discovering alternative solvents that are eco-friendly and can either boost the efficacy or substitute this solvent for extracting CO_2 from flue gas or natural gas.

Recent studies have revealed the promising potential of amino acid salt (AAS) as an alternative solvent. AAS solvents exhibit identical amine functionality, high chemical reactivity with CO_2, better resistance towards degradation, and low volatility, and they are environmentally friendly [31–35]. Another unique feature of AAS is its ability to form a solid precipitate during reaction with CO_2. The formation of the precipitate facilitates the enhancement of the CO_2 absorption capacity of AAS and creates opportunities for

temporary CO_2 storage [36]. The reaction of AAS with CO_2 is similar to alkanolamines [6], which will be further discussed in Section 2. Hamzehie et al. [37] reported the stability of potassium glycinate towards oxidation, whereby the CO_2 loading was consistent between 1.924 and 1.931 mol CO_2/mol solvent even after 2 h of exposure to pure oxygen. Hence, this finding signifies the strong resistance of amino acids towards oxidative degradation. In addition, AAS solvents also show superior reactivity towards CO_2 compared to amine solvents owing to their higher pKa values [38]. The high surface tension of AAS also facilitates the chemical binding of CO_2, which contributes to its favorable CO_2 absorption capacity. Despite their advantages, AAS solvents are susceptible to precipitation during absorption, especially at a high concentration of CO_2, which may restrict mass transport or lead to equipment damage [39]. From another perspective, the formation of solid precipitation may also have a positive effect by reducing the energy requirements for solvent regeneration and increasing CO_2 loading, provided that the process is intensively controlled [40]. In addition, AAS also usually exhibits a lower absorption rate than amine, mainly due to the presence of bulk substituent groups attached to the amino acids. Hence, these limitations create an area of improvement to cultivate innovative solutions to enhance the practicability of AAS for CO_2 removal. Generally, AASs are classified into four main groups based on their side chains: linear amino acids, poly amino acids, cyclic amino acids, and sterically hindered amino acids (SHAAs) [41].

Aftab et al. [42] reported the performance of sodium β-alaninate (Na-βala), a linear-type AAS for CO_2 removal, using a concentration that ranged between 10 and 30 wt.%. The experimental findings demonstrated that the CO_2 loading capacity decreased as the Na-βala concentration and operating temperature increased. In addition, the authors also discovered that 30 wt.% Na-βala exhibits a higher CO_2 loading capacity than 30 wt.% MEA at the temperature of 313.1 K. This finding can be attributed to the unstable carbamate formation during the reaction between Na-βala with CO_2. The carbamate ion may easily hydrolyze into bicarbonate and liberate free amines, promoting CO_2 absorption. Chang et al. [43] investigated CO_2 solubility in aqueous potassium salt solutions L-prolinate (KPr) and DL-aminobutyrate (KAABA) at temperatures of 313.2, 333.2m and 353.2 K and CO_2 partial pressures up to 1000 kPa. The measured salt concentrations were studied at 7.5, 14.5, and 27.4 wt.% for KPr solutions and 6.9, 13.4, and 25.6 wt.% for KAABA solutions, respectively. KAABA solutions showed consistently higher CO_2 loadings at high pressures than the loadings in KPr solutions. The steric character of the methyl group (-CH_2CH_3) in KAABA reduces the stability of the formed carbamate. Thus, the carbamate can undergo hydrolysis to form bicarbonate, releasing free amine and enhancing CO_2 loading. Unlike KAABA, the reaction of CO_2 with KPr tends to form stable carbamate. However, if the pH is favorable, the carbamate may undergo hydrolysis to form bicarbonate.

Among the various types of AAS, SHAA has been remarked as one of the potential candidates for CO_2 removal due to the presence of steric hindrance, which offers higher CO_2 loading capacity and lower thermal energy demand for regeneration. According to Satori and Savage [44], SHAA refers to a tertiary amino acid in which its primary or secondary carbon atom is attached to the amino acid. L-Cysteine (CYS) is one of the SHAAs that can be used as a potential solvent for CO_2 removal. The presence of the steric effect in SHAA reduces the stability of the formed carbamate. Consequently, the unstable carbamate may undergo hydrolysis to form bicarbonate and free amine molecules, thereby promoting CO_2 absorption. CYS has a bulky group (-SH) that lies at the second carbon (β-carbon), and it is considered to have good performance in absorption and desorption compared to other amino acids. According to Song et al. [41], CYS showed a lower initial absorption rate and higher initial desorption rate compared to other amino acids such as alanine (ALA), taurine (TAU), diglycine (DIGLY), glutamine (GLN), asparagine (ASN), and pyroglutamic acid (PGA), as shown in Table 1. Referring to Table 1, the net cyclic capacity of CYS is also comparable to other linear amino acid salts (glycine, taurine, β-alanine, and γ-aminobutyric acid). These attributes make CYS a favorable candidate for CO_2 removal due to its excellent desorption performance that leads to lower energy requirements to desorb CO_2 and reduce

solvent regeneration costs. To date, very few studies are available on the performance of CYS for CO_2 removal. The compelling characteristics and performance of CYS drive out the interest to further explore the potential of CYS as a green solvent and an alternative to amine solvents for CO_2 removal. Currently, the performance of CYS has only been reported for corrosion inhibition and biomedical applications.

Table 1. Cyclic CO_2 absorption and desorption properties of MEA and various AAS [41].

Absorbents	Concentration (kmol/m^3)	Initial Absorption Rate (mol CO_2/(mol. amine. min))	Net Cyclic Capacity (mol CO_2/(mol. amine. min))	Initial Desorption Rate (mol CO_2/(mol. amine. min))
Monoethanolamine (MEA)	1	3.84×10^{-2}	2.00×10^{-2}	0.483
Cysteine (CYS)	1	3.18×10^{-2}	2.46×10^{-2}	0.485
Alanine (ALA)	1	3.16×10^{-2}	1.98×10^{-2}	0.535
Taurine (TAU)	1	3.17×10^{-2}	2.26×10^{-2}	0.483
Diglycine (DIGLY)	1	2.99×10^{-2}	2.18×10^{-2}	0.467
Glutamine (GLN)	1	3.06×10^{-2}	2.08×10^{-2}	0.535
Asparagine (ASN)	1	2.79×10^{-2}	2.34×10^{-2}	0.547
Pyroglutamic acid (PGA)	1	2.41×10^{-2}	0.38×10^{-2}	0.069

The fundamentals of the physicochemical property data are useful for the design, simulation, and operation of the CO_2 removal process [45]. According to Garg et al. [46], the density and viscosity of the absorbent are crucial in the process equipment design as they may affect the hydrodynamics and mass transfer. Furthermore, these properties are essential in determining the reaction rate constant and gas diffusivities. On the other hand, refractive index (RI) data are beneficial for the verification of solvent purity and the identification of solvent composition [46,47]. Moreover, RI data are also useful for the derivation of molar refraction, which is essential for comprehending the molecular arrangement and interaction within the solvent system under different concentrations and temperatures [18,48]. Subsequently, these qualities will facilitate the understanding of the behavior and properties of the solvent. For instance, Rahim et al. [49] estimated the electronic polarizability or molar refraction of a solvent based on RI data, which is an important parameter to determine the free volume available in the solvent. Therefore, it is worthwhile to investigate the RI to obtain useful insight into the gas solubility in the solvent. To the best of our knowledge, there are no available data in the open literature on the physicochemical properties of the aqueous potassium salt of cysteine (K-CYS). Therefore, the physicochemical properties such as density, viscosity, and refractive index were studied and are reported in this paper. All properties were measured over a temperature range from 298.15 to 333.15 K and concentrations from 5 to 30 wt.%. The CO_2 solubility in K-CYS solutions was also evaluated at different temperatures between 303.15 K and 333.15 K, and operating pressures up to 20 bar were also provided. The study of CO_2 solubility is crucial to assess solvent performance.

2. Reaction Mechanisms

2.1. Amino Acid Solvent (AAS)

According to He et al. [50], the reaction between CO_2 and aqueous amino acid solvent (AAS) generally occurs via zwitterion mechanisms, as shown below. In water, amino acids exist in a zwitterion form whereby the molecules present as electrically neutral and less reactive towards CO_2 [51]. Hence, the addition of a strong base such as sodium or potassium hydroxide is necessary to increase the reactivity of the AAS towards CO_2. Referring to Figure 1, the aqueous AAS chemically reacts with CO_2, forming an unstable carbamate. The formed carbamate typically hydrolyzes into deprotonated amino acid and carbonate, which provides more free amines to react with CO_2, as shown in Figure 2 [32]. The extent of carbamate hydrolyzation depends on the concentration of the aqueous AAS, the solution pH, and the stability of carbamates [51].
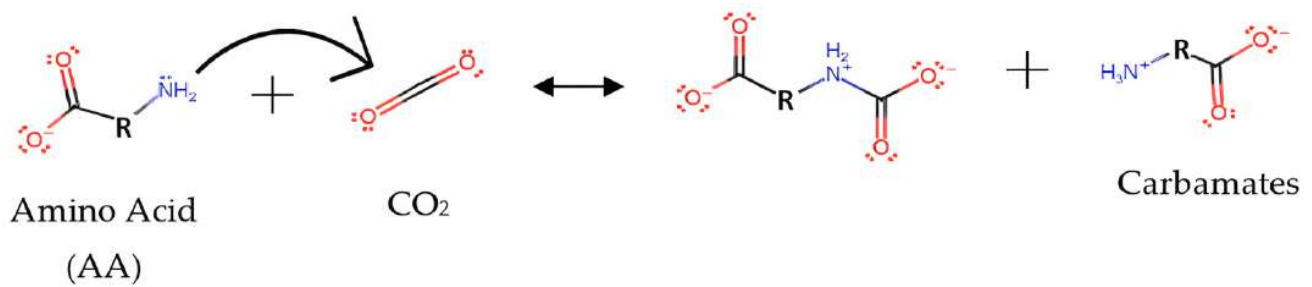
Figure 1. Reaction mechanism between amino acid (AA) with CO_2. R refers to the amino group.
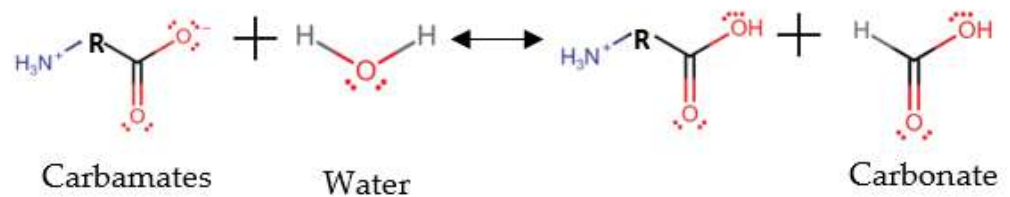

Figure 2. Hydrolysis of carbamates.

2.2. Alkanolamines

Similarly, the reaction mechanisms of alkanolamines, such as MEA with CO_2, also yields carbamate, as shown below. CO_2 absorption using amine-based solvents involves a series of reactions, as illustrated in Figures 3 and 4 [35]. In Figure 3, the amine acts as a weak base, which reacts with acidic CO_2 to form carbamate. In the presence of moisture, this carbamate further reacts to form bicarbonate, as shown in Figure 4. Based on this mechanism, the majority of absorbed CO_2 in the liquid amine will result in the formation of bicarbonate. The interaction between the absorbent and CO_2 can be weakened by increasing the temperature or reducing the pressure of the solution. This causes the CO_2 to be separated from the amine solvent, thereby regenerating the solvent for future use [24]. Contrary to the AAS, the carbamates and bicarbonate created by MEA are relatively stable, thereby increasing the energy required for regeneration [51].
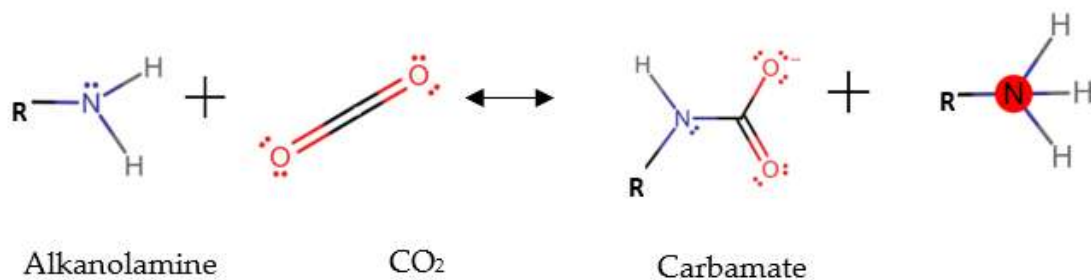

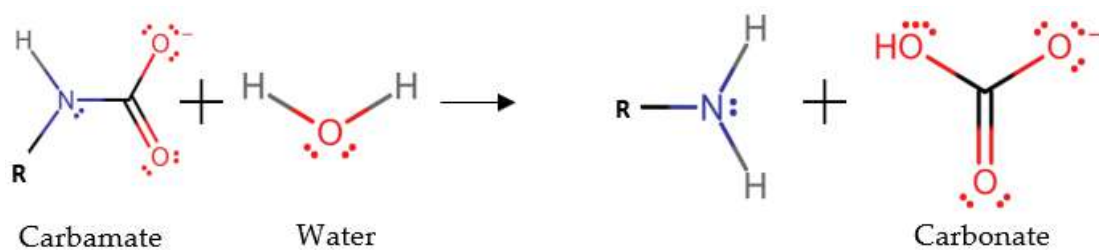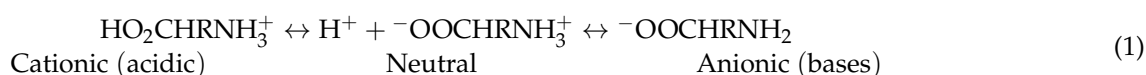**Figure 3.** Reaction mechanism between alkanolamines with CO_2. R refers to the alkyl group [35].

Figure 4. Hydrolysis of carbamate into bicarbonate [35].

3. Methodology

3.1. Chemicals and Materials

L-Cysteine (CYS) with $\geq$99% purity and potassium hydroxide (KOH) with $\geq$85% purity were purchased from Merck. The chemicals were used as delivered without further purification. K-CYS salt solutions were prepared by neutralizing CYS with an equimolar amount of KOH and deionized water (99% pure), following the procedure from the literature [16,18]. All weight measurements were carried out using an electronic analytical balance (Sartorius, Model: BSA224S-CW, Goettingen, Germany) with $\pm 10^{-4}$ g accuracy.

In water, amino acids exist as zwitterions with a protonated amino group (-NH$_3{}^+$), which does not favor CO$_2$ [52]. Hence, the deprotonation of the zwitterions is essential to increase the reactivity of amino acids towards CO$_2$ [31].

$$HO_2CHRNH_3^+ \leftrightarrow H^+ + {}^-OOCHRNH_3^+ \leftrightarrow {}^-OOCHRNH_2 \tag{1}$$
Cationic (acidic)   Neutral   Anionic (bases)

The addition of KOH as the strong base aims to deprotonate the amino group (-NH$_3{}^+$) and make it reactive towards carbon dioxide (CO$_2$) [52].

$$^-OOCHRNH_3^+ + KOH \rightarrow KO_2CHRNH_2 + H_2O \tag{2}$$

The physicochemical properties of prepared aqueous solutions with different concentrations of 5, 10, 20, and 30 wt.% were measured over the temperature range from 298.15 K to 333.15 K. The chemical structure, molecular formula, molar mass, and source of the chemicals used are presented in Table 2.

Table 2. The chemical structure, molecular formula, purity, molar mass, and source of the chemical used.

Component	Molecular Formula	Purity, %	Molar Mass, g	Source
L-Cysteine	C$_3$H$_7$NO$_2$S	$\geq$99	121.16	Merck
Potassium hydroxide	KOH	$\geq$85	56.11	Merck
Water	H$_2$O	99	18.02	-

3.2. Density Measurement

The density of K-CYS solutions was measured using a digital oscillating tube densimeter (Anton Paar, DMA-4500 M, Graz, Austria) with $\pm 5 \times 10^{-5}$ g cm^{-3} accuracy. Before the measurement, the tube was first cleaned with acetone and dried with air to avoid sample contamination. The instrument was then calibrated using deionized water to ensure reliable experimental data. The density measurement procedure can also be found in the literature [9,53]. The density values of each sample were measured in triplicate, and the average values were reported. The uncertainty of density and temperature was $\pm 6 \times 10^{-5}$ g cm^{-3} and ± 0.01 K, respectively.

3.3. Viscosity Measurement

The viscosity of the aqueous solutions of K-CYS was measured using a digital rolling ball viscometer (Anton Paar, Model: Lovis-2000 M/ME, Graz, Austria) with a stated accuracy of ± 0.5%. Firstly, the capillary was adequately cleaned with acetone and dried with air to avoid contamination. Before each measurement, the equipment was calibrated with deionized water to achieve accurate measuring results. During the sample injection into the suitable capillary, the tube should be free from the air bubbles to prevent any interruption in the ball movement resulting in inaccurate results. The viscosity measurement was based on the rate of the ball rolling through the liquid samples between the marks in the liquid-filled capillary [53]. The capillary was kept inclined at an angle between 10° and 80°. The viscosity of each sample was measured in the unit of mPa s by taking the average of

three measurements. The uncertainty of viscosity and temperature was $\pm 7 \times 10^{-3}$ mPa s and ± 0.02 K, respectively.

3.4. Refractive Index Measurement

The refractive index of K-CYS was measured at different temperatures between 298.15 and 333.15 K using a digital Anton Paar refractometer (Model: WR Abbemet, Graz, Austria) with the accuracy of $\pm 4 \times 10^{-5}$ n_D. The refractometer was operated at wavelength, $\lambda = 589.3$ nm. The refractometer was calibrated using deionized water to ensure measurement accuracy. Prior to each measurement, it is necessary to clean the prism with acetone and deionized water to avoid sample contamination and errors during the measurement of the refractive index. The description of the measurement procedure is also given elsewhere in the literature [46,47,51]. The refractive index of the aqueous K-CYS solution was reported in the unit of n_D by taking the average of 3 measurements at different concentrations and temperatures. The uncertainties of the refractive index and temperatures were estimated to be $\pm 5 \times 10^{-5}$ n_D and ± 0.03 K, respectively.

3.5. CO$_2$ Loading Capacity Measurement

The experimental setup used in this work is shown in Figure 5. The solubility of CO_2 in aqueous solutions was measured using SOLTEQ High-Pressure Gas Solubility Cell (Model: BP-22, Vantaa, Finland). A similar experimental setup was also reported by [42,54]. The unit comprises two main vessels, a mixing vessel (MV) and an equilibrium cell (EC), with 3 L and 50 mL capacity, respectively. The gas vessel was used for CO_2 storage. Meanwhile, the equilibrium cell (EC) acts as the chamber for mixing and reaction between the gas and solvent. Both vessels were thermo-regulated using an electric water bath, the JULABO thermostatic bath, set at the required temperatures with an accuracy of ± 0.1 °C.

Figure 5. Experimental setup for CO$_2$ solubility study [55].

Prior to the experiment, both vessels were first purged with nitrogen gas to remove any trapped unwanted gas or contaminants. Next, CO_2 was pressurized in MV up to the desired pressure using an air-driven booster pump. Both vessels, MV and EC, were equipped with a digital pressure sensor (Model: Druck DPI 150) with an accuracy of

± 1.0 kPa, as well as a temperature transmitter (Model: Yokogawa 7653) with an accuracy of ± 0.1 K). Prior to injecting CO_2 into EC, the initial pressure and temperature of MV were recorded as P1 and T, respectively. Subsequently, approximately 6 mL of the aqueous K-CYS solution was introduced into the EC using a metering pump. The vapor pressure, Pvap, at a given temperature was recorded. As the pressure and temperature in EC reached a stable condition, CO_2 was fed into the EC from MV. The pressure inside EC after the CO_2 injection was recorded as P2. Furthermore, the aqueous solution in EC was constantly agitated at 300 rpm by using the magnetic stirrer at the bottom of EC to enhance the rate of mass transfer. Upon reaching equilibrium, the final pressure, Peq, and temperature, Teq, in the EC were recorded. The process parameters, such as pressure and temperature, were recorded in the data acquisition system every second until equilibrium was achieved. The experiments were carried out at 3 different temperatures: 303.15, 313.15, and 333.15 K with an operating pressure of CO_2 in the range of 2 to 20 bar (g). Upon attaining a steady state, the CO_2 solubility in aqueous K-CYS was acquired in terms of CO_2 loading, which refers to the number of moles of CO_2 absorbed per moles of solvent. The equation used to determine the CO_2 solubility was further discussed in the following sections.

3.6. CO_2 Loading Capacity Calculation

In this work, the solubility of CO_2 in the solvent was evaluated via the pressure decay method, whereby the amount of CO_2 absorbed in the solvent was determined based on the changes in pressure [25,56,57]. The unique feature of this method is that the analysis of the liquid phase is not necessary. The number of moles of CO_2 transferred from the MV into the EC can be obtained from Equation (3):

$$n_{CO_2} = \frac{V_T}{RT}\left(\frac{P_1}{Z_1} - \frac{P_2}{Z_2}\right) \tag{3}$$

where V_T is the volume of the reactor (MV), P_1 and P_2 are the initial and the final pressure of MV, Z_1 and Z_2 are the compressibility factors, R represents the real gas constant, and T is the operating temperature. The Peng–Robinson equation of state (EOS) was used in calculating the compressibility factors.

Equilibrium partial pressure of CO_2 in the system, P_{CO_2}, was calculated by using Equation (4):

$$P_{CO_2} = P_T - P_V \tag{4}$$

where P_T denotes the total pressure, and P_V represents the vapor pressure of the liquid samples. In these calculations, the vapor pressure of amino acid P_v can be neglected as it is minimal ($P_v = 6.73 \times 10^{-7}$ mmHg at 25 °C) [58].

The moles of the unabsorbed CO_2 in the gas phase were calculated by using Equation (5):

$$n^g_{CO_2} = \frac{V_g P_{CO_2}}{Z_{CO_2} RT} \tag{5}$$

where V_g is the gas-phase volume of the equilibrium cell, Z_{CO_2} is the compressibility factor at P_{CO_2}, and T is the temperature inside the EC.

The effective number of moles of dissolved CO_2 in the liquid phase, $n^l_{CO_2}$, is calculated from the difference between the number of moles of CO_2 (n_{CO_2}) transferred from the gas vessel to EC and the number of moles of CO_2 present in the gaseous phase at the equilibrium state ($n^g_{CO_2}$).

$$n^l_{CO_2} = n_{CO_2} - n^g_{CO_2} \tag{6}$$

Then, the mole of amino acid salt is calculated using Equation (7).

$$n_{AM} = \frac{\rho V_1 m}{M} \tag{7}$$

where ρ is the density of the aqueous amino acid salt solution, V_1 is the solvent volume used for absorption (differential volume), m is the mass fraction, and M is the molecular weight of the amino acid used.

The CO_2 solubility was thus expressed in terms of the molar fraction by Equation (8).

$$\alpha = \frac{n^l_{CO_2}}{n_{AM}} \tag{8}$$

where α is the solubility in terms of CO_2 loading as per mole of CO_2 absorbed in the solvent ($n^l_{CO_2}$) per mole of amino acid salt (n_{AM}).

4. Results and Discussions

4.1. Physicochemical Properties

To validate the experimental data, the analytic tools were calibrated by measuring the density (ρ), viscosity (η), and refractive index (n_D) of pure water at three different temperatures of 298.15, 303.15, and 308.15 K. The results obtained were compared with data from the literature [59]. The compared results for all properties of pure water are presented in Table 3. The absolute relative deviation (ARD%) implies the data reliability and demonstrates the deviation between experimental and literature values. ARD% was calculated by using Equation (9).

$$\text{ARD}, \% = \frac{1}{n}\sum \left| \frac{X_{\exp} - Y_{lit}}{Y_{lit}} \right| 100 \tag{9}$$

where n is the number of experimental data points, X_{exp} refers to the experimental, and Y_{lit} refers to the literature values. As shown in Table 3, the measured density, viscosity, and refractive index of pure water are in good agreement with the reported values in the literature [59].

Table 3. Comparison of experimental data of density, ρ, viscosity, η, and refractive index, n_D, of pure water with the literature data [59].

T/K	This Work	Literature [59]	ARD, %
		ρ/g cm^{-3}	
298.15	0.99739	0.997113	
303.15	0.99599	0.995720	0.028
308.15	0.99438	0.994105	
T/K		η/mPa s	
298.15	0.897	0.890	
303.15	0.805	0.797	1.049
308.15	0.729	0.719	
T/K		n_D	
298.15	1.33285	1.33268	
303.15	1.33230	1.33211	0.014
308.15	1.33166	1.33148	

Tables 4–6 show the measured values of the density, viscosity, and refractive index of aqueous K-CYS salt solutions at each temperature. Based on Table 4, the density of the K-CYS solution decreases when the temperature increases from 298.15 K to 333.15 K. This finding can be attributed to the high mobility of molecules in the aqueous solution at elevated temperatures as the molecules gained more kinetic energy. Consequently, the rising temperature leads to the disruptions of hydrogen bonding and the weakening of intermolecular forces within the aqueous solution, causing the separation of molecules away from each other [31,45,60]. As the intermolecular interaction within the aqueous solution

weakened, the solution volume increased and subsequently resulted in the reduction of density [61,62]. On the contrary, the increment in the concentration of K-CYS leads to a higher density due to the increased number of molecules in the aqueous solutions and intermolecular forces between the molecules. The densities of the K-CYS solutions were obtained in the range of 1.00454 to 1.14510 g cm^{-3}. Similar trends were also observed by other researchers [31,59,60,63,64].

Table 4. Experimental values of densities, ρ, of aqueous K-CYS solution at different mass fractions, w, and temperatures, T.

Temperature, T (K)	Density, ρ (g cm^{-3})			
	Mass Fractions, w			
	5 wt.%	10 wt.%	20 wt.%	30 wt.%
298.15	1.01956	1.04292	1.09130	1.14510
303.15	1.01794	1.04107	1.08904	1.14247
308.15	1.01611	1.03905	1.08665	1.13973
313.15	1.01412	1.03687	1.08412	1.13687
318.15	1.01195	1.03453	1.08146	1.13390
323.15	1.00963	1.03206	1.07868	1.13082
328.15	1.00715	1.02944	1.07578	1.12763
333.15	1.00454	1.02670	1.07277	1.12435

Table 5. Experimental values of viscosities, η of aqueous K-CYS solution at different mass fractions, w, and temperatures, T.

Temperature, K	Viscosity, η (mPa s)			
	Mass Fractions, w			
	5 wt.%	10 wt.%	20 wt.%	30 wt.%
298.15	0.901	0.984	1.264	1.685
303.15	0.811	0.885	1.138	1.502
308.15	0.733	0.799	1.032	1.348
313.15	0.666	0.725	0.947	1.215
318.15	0.610	0.662	0.865	1.103
323.15	0.560	0.608	0.769	1.006
328.15	0.519	0.563	0.707	0.922
333.15	0.482	0.521	0.654	0.849

Table 6. Experimental values of refractive indices, n_D, of aqueous K-CYS solution at different mass fractions, w, and temperatures, T.

Temperature, K	Refractive Index, n_D			
	Mass Fractions, w			
	5 wt.%	10 wt.%	20 wt.%	30 wt.%
298.15	1.34176	1.35141	1.37153	1.39329
303.15	1.34096	1.35067	1.37055	1.39209
308.15	1.34021	1.34993	1.36960	1.39095
313.15	1.33946	1.34905	1.36871	1.38991
318.15	1.33873	1.34828	1.36796	1.38921
323.15	1.33800	1.34756	1.36743	1.38883
328.15	1.33729	1.34693	1.36708	1.38861
333.15	1.33704	1.34624	1.36684	1.38859

Table 5 shows that the viscosity of K-CYS solutions increases at higher solvent concentrations. For instance, at the temperature of 298.15 K, the viscosity increases from 0.901 mPa s to 1.685 mPa s with the increasing concentration of K-CYS from 5 wt.% to

30 wt.%. This finding is attributed to the higher molecular resistance in a more concentrated solution [65]. However, the viscosity reduces at rising temperature, as shown in Table 5, whereby the viscosity of 30 wt.% aqueous K-CYS solution significantly descends from 1.685 mPa s to 0.849 mPa s as the temperature rises from 298.15 K to 333.15 K. The decrement in viscosity at higher temperatures was due to the decrease in electrostatic interaction of the molecules and the availability of more free spaces between the molecules [64]. Hence, the internal resistance of molecules decreased and subsequently reduced the viscosity. Similar trends were also observed in different solvent systems [18,63,66,67]. On the other hand, aqueous K-CYS solution also exhibits lower viscosity compared to the conventional solvents MEA and MDEA reported in the literature. For instance, at T = 313.15 K and the same concentration of 30 wt.%, the viscosity of aqueous K-CYS is 1.685 mPa s, which is lower than MEA [66] and MDEA [68], the viscosities of 2.52 mPa s and 1.93 mPa s, respectively. The significant difference in the viscosity shown by the aqueous K-CYS solution implies that this solvent offers a lower mass transfer resistance compared to the conventional solvents. Hence, this would facilitate the solvent pumping and minimize the energy required for the process, which consequently may contribute to cost savings.

Referring to Table 6, the refractive indices of the K-CYS solutions increase as the concentration increases from 5 wt.% to 30 wt.%. At 298.15 K, the refractive index, n_D, of the K-CYS solution remarkably increases from 1.34176 to 1.39329 with increasing solvent concentrations. The increment in the refractive index at high concentrations is due to the rising number of molecules being struck by the light from the refractometer [51,69]. On the other hand, an opposite trend was observed at an ascending temperature from 298.15 to 333.15 K, where, at a constant solvent concentration of 30 wt.%, n_D gradually decreases from 1.39329 to 1.38859. The vibration among the molecules increased at higher temperatures and created more spaces between the molecules. Hence, a lower number of molecules were struck by the light from the refractometer, which eventually resulted in the reduction of refractive index values [47,60]. Similar trends were also reported by other researchers [18,45,47].

4.2. Correlation Study

To date, various empirical expressions have been developed to correlate density, viscosity, and refractive index with temperature. Using a similar approach by Murshid et al. [53], the experimental data for density were correlated with temperature using a linear equation in Equation (10).

$$\rho = A_0 + A_1 T \tag{10}$$

where ρ is the density (g/cm^3), A_0 and A_1 are the correlation parameters, and T is the temperature (K). A_o and A_1 were obtained using the least-squares method. Meanwhile, the standard deviations (SDs) for density were calculated by using Equation (11):

$$SD = \left[\frac{\sum_i^n \left(X_{\text{exp}} - X_{corr.} \right)^2}{n} \right]^{0.5} \tag{11}$$

where X_{exp} is the experimental value of the density, X_{corr} is the correlated value of the density, and n is the number of data points. The correlation parameters and *SD* for the density of K-CYS are given in Table 7.

Table 7. Correlation parameters and SD for densities of different mass fractions of aqueous K-CYS.

wt.%	A_0	$10^4 A_1$	R^2	10^{-4} SD
5	1.14844	−4.30254	0.99424	3.84
10	1.18186	−4.64214	0.99591	3.47
20	1.24973	−5.29863	0.99778	2.90
30	1.32233	−5.93119	0.99863	2.54

Figure 6 shows the parity plot between the experimental and predicted density of aqueous K-CYS solution at the different mass fractions. The black line in Figure 2 represents the correlated density. Based on Figure 2, the correlation is well fitted to the data with $R^2 \geq 0.99424$, indicating satisfactory agreement between the experimental and predicted density. In addition, this finding was also supported by the relatively low standard deviation of less than 0.000384.
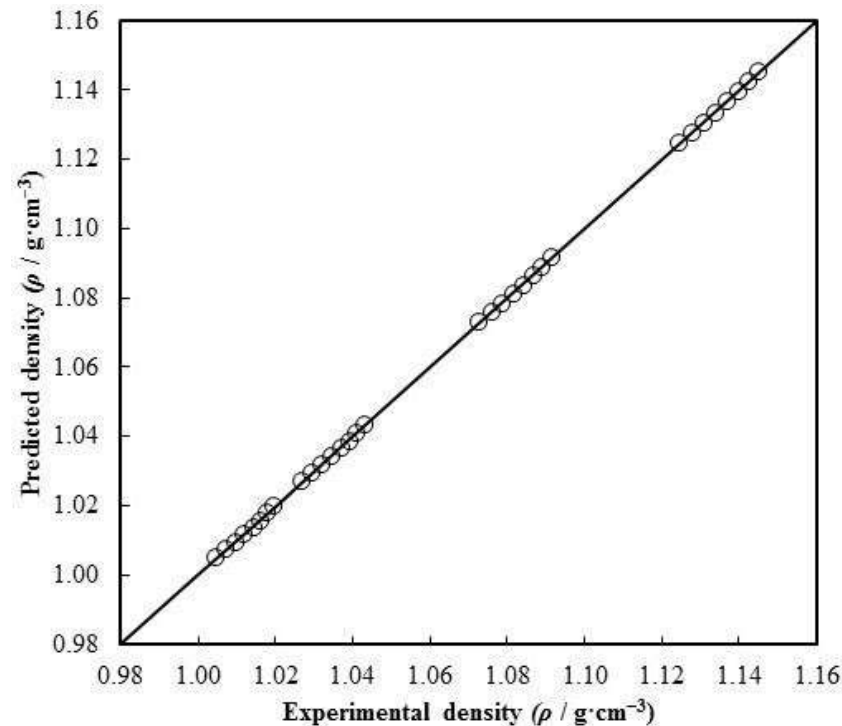

Figure 6. Comparison between experimental and correlated values of density of aqueous K-CYS.

On the other hand, the thermal expansion coefficient (α_P) is a crucial property in the industrial design of CO_2 separation systems [45]. The experimental density data were used to estimate α_P, where Equation (12) was used to calculate the thermal expansion coefficient of K-CYS solutions at different concentrations and temperatures [45,70].

$$\alpha_P = -\left(\frac{1}{\rho}\right)\left(\frac{\delta\rho}{\delta T}\right)_P = -\frac{A_1}{A_0 + A_1 T} \tag{12}$$

where α_P is the thermal expansion coefficient, ρ is the density, T is the temperature, and A_0 and A_1 are the fitting parameters obtained from Equation (10).

The thermal coefficient data of the K-CYS solution at different mass fractions and temperatures are listed in Table 8. The thermal expansion coefficient increased linearly from 4.21×10^{-4} to 5.27×10^{-4} K^{-1} with increasing temperature and concentration. A slight increment in the thermal expansion coefficient values shows that the volume of the solution does not change significantly with the temperature rise. Similar behaviors were also reported in the literature for various aqueous systems [45,63,67].

For viscosity, the measured data were correlated with temperature using an exponential equation in Equation (13).

$$\eta = B_0 \exp(-B_1 \cdot T) \tag{13}$$

where η represents viscosity (mPa s), B_0 and B_1 refer to the correlation coefficients, and T is the temperature (K). B_0 and B_1 were obtained by using the least-squares method. The correlation coefficients and SD are given in Table 9.

Table 8. Thermal expansion coefficient of different mass fractions of aqueous K-CYS.

T/K	$\alpha_P/10^{-4}$ K^{-1}			
	w = 5 wt.%	*w* = 10 wt.%	*w* = 20 wt.%	*w* = 30 wt.%
298.15	4.21	4.45	4.85	5.18
303.15	4.22	4.46	4.87	5.19
308.15	4.23	4.47	4.88	5.20
313.15	4.24	4.48	4.89	5.22
318.15	4.25	4.49	4.90	5.23
323.15	4.26	4.50	4.91	5.24
328.15	4.27	4.51	4.93	5.26
333.15	4.28	4.52	4.94	5.27

Table 9. Correlation parameters and SD for viscosities of different mass fractions of aqueous K-CYS.

wt.%	$10^{-2} B_0$	$10^2 B_1$	R^2	10^{-3} SD
5	1.81990	−1.78691	0.99599	8.95
10	2.16775	−1.81577	0.99638	9.41
20	3.58453	−1.89658	0.99851	6.98
30	5.61252	−1.95472	0.996849	16.11

Figure 7 shows the parity comparison between the experimental and predicted viscosity of the K-CYS solution at different temperatures. The predicted viscosity of K-CYS is indicated by the black line in Figure 3. As shown in Figure 3, the predicted viscosity was found good-fitted to the experimental data with $R^2 \geq 0.99$ and SD ≤ 0.016.
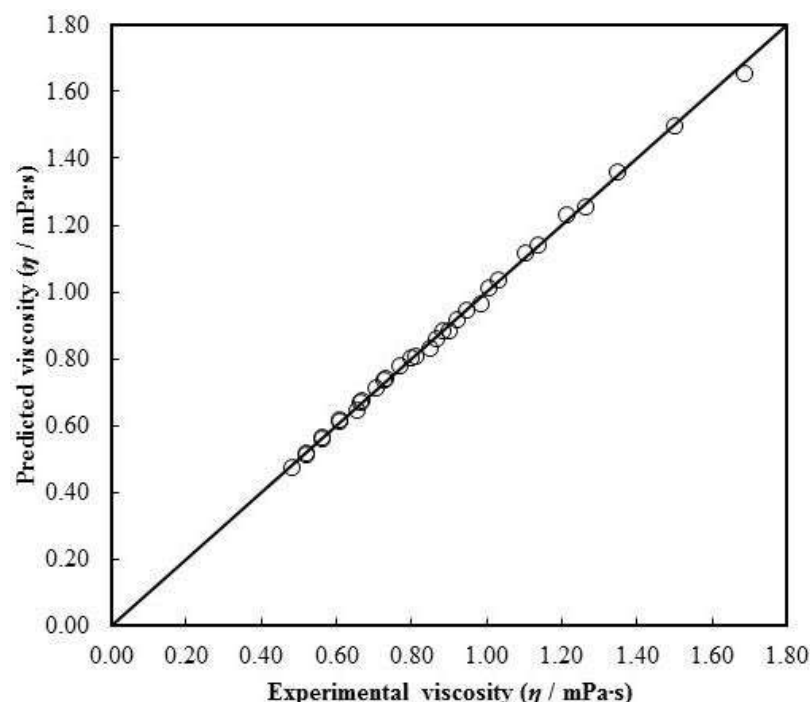
Figure 7. Comparison between experimental and correlated values of viscosity of aqueous K-CYS.

The activation energy ($E\eta$) is a potential barrier to be overcome to allow the mobilization of solvent molecules. Hence, the quantitative analysis of the viscosity activation energy is significant in assessing the fluidity of the solvents. Moreover, the $E\eta$ of viscosity is also an essential parameter that reflects the sensitivity of viscosity towards temperature changes. In the present work, the experimental viscosity data were further used to calculate

the activation energies at different concentrations using a logarithmic form of the Arrhenius equation, as expressed in Equation (14).

$$Ln\eta = ln\eta\infty - \frac{E_\eta}{RT} \qquad (14)$$

where η is the viscosity, η_∞ is the infinite-temperature viscosity, $E\eta$ is the activation energy, R is the gas constant (0.00831 kJ mol^{-1} K^{-1}), and T is the temperature. The graph of $ln\eta$ versus $1/T$ is plotted as shown in Figure 3. $E\eta$ is estimated based on the gradient of the Arrhenius plot in Figure 8.
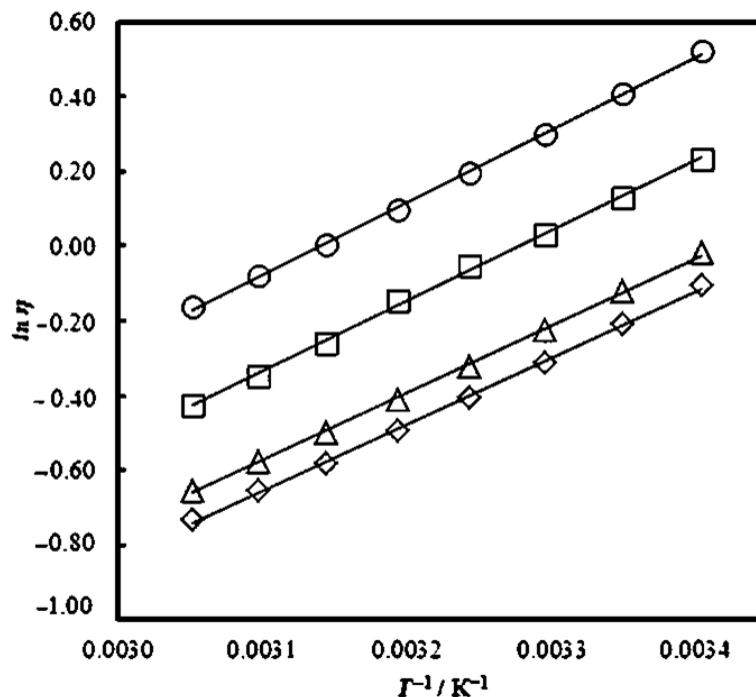
Figure 8. The relationship of $ln\eta$ and temperature reciprocal for different mass fractions of aqueous K-CYS: (◇) 5 wt.%; (△) 10 wt.%; (□) 20 wt.%; (○) 30 wt.%.

The calculated values of the activation energy and the infinite-temperature viscosity of the aqueous K-CYS solutions are presented in Table 10. In the present work, the estimated activation energies of K-CYS solutions ranged from 14.77545 to 16.15941 kJ mol^{-1}. Based on Table 10, the activation energy ($E\eta$) increases in the order of 30 wt.% > 20 wt.% > 20 wt.% > 5 wt.%. The finding indicates the sensitivity of activation energy with the changes In solvent concentration. The increase in concentration leads to an increase in activation energy, which might be due to the stronger interactions between the molecules in the solvents, thus increasing the potential barrier for the molecules to move past each other. Similar trends were also observed for different types of solvents [71,72].

Table 10. Calculated activation energies and infinite-temperature viscosities at different mass fractions of K-CYS.

wt.%	$E\eta$/kJ mol^{-1}	η^∞/mPa s
5	14.77545	2.29551×10^3
10	15.01246	2.28041×10^3
20	15.65887	2.28292×10^3
30	16.15941	2.45753×10^3

For the refractive index, the experimental data were correlated by the least-squares method as a function of temperature by using Equation (15). The best fit for the refractive index was a polynomial equation, and the coefficients are reported in Table 11.

$$n_{\mathrm{D}} = C_0 + C_1 T + C_2 T^2 \tag{15}$$

where n_{D} is the refractive index; C_0, C_1, and C_2 are the fitting parameters; and T is the temperature.

Table 11. Correlation parameters and SD for refractive indices of different mass fractions of aqueous K-CYS.

wt.%	C_0	$10^4\,C_1$	$10^6\,C_2$	R^2	10^4 SD
5	1.48364	−7.76223	1.00786	0.99727	2.30
10	1.44308	−4.48605	0.47387	0.99934	3.90
20	1.69046	−19.04114	2.79937	0.99911	0.80
30	1.88146	−29.79979	4.50405	0.99866	4.10

Figure 9 demonstrates the parity plot of comparison between the predicted and experimental refractive index of K-CYS at different mass fractions and temperatures. The predicted data of the refractive index are indicated by the black lines. A good consistency was observed between the experimental and predicted refractive index data of K-CYS solutions with SD ≤ 0.00041. Conclusively, the applied empirical correlation is observed to be reliable for the estimation or interpolation of the refractive index of K-CYS solution under different temperature and mass fractions.
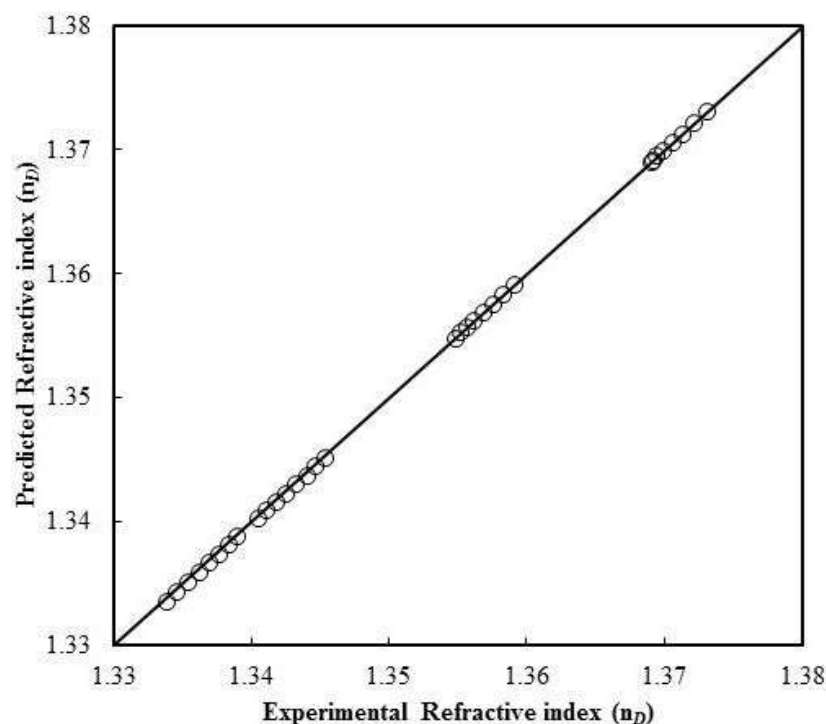

Figure 9. Comparison between experimental and predicted values of the refractive index of aqueous K-CYS.

4.3. CO$_2$ Loading Capacity Study

A CO_2 solubility study is essential to evaluate the performance of the solvents and assess their feasibility for practical application in the industry. The equilibrium data of the solvent are crucial in designing the absorption system for CO_2 removal. The solubility of CO_2 was typically investigated in terms of CO_2 loading, which can be expressed as mol CO_2 absorbed per mol of solvent. In the present work, the operating conditions were selected based on the industrial implementation of amine-based absorption technology. Prior to

the experiment, the high-pressure solubility cell was first calibrated by using 30 wt.% of aqueous MEA at 313.15 K to ensure the measurement accuracy. The CO_2 loading of MEA was compared with the literature data, as shown in Table 12. The average absolute relative deviation (%ARD) of the results obtained was calculated based on Equation (9). Based on Table 12, a good agreement was found between experimental and literature data with the %ARD of 0.9173%. Hence, this finding signifies the reliability of the experimental results reported in this work.

Table 12. A comparison of CO_2 solubility in 30 wt.% aqueous MEA solution at 313.15 K.

Present Work		Literature [73]		% ARD
α (mol of CO_2/mol of MEA)	P_{CO_2} (bar (g))	α (mol of CO_2/mol of MEA)	P_{CO_2} (bar (g))	
0.703	8.56	0.728	8.83	
0.731	10.03	0.763	12.56	0.9173
0.759	13.08	0.772	15.80	
0.806	19.20	0.806	19.73	

4.3.1. Effect of Pressure

Table 13 summarizes the experimental CO_2 loading of aqueous K-CYS solution measured at different pressure, temperatures, and mass fractions. The solubility of CO_2 in the aqueous solutions was investigated at different pressures between 2 bar (g) and 20 bar (g) and temperatures of 303.15 K, 313.15 K, and 333.15 K. Referring to Table 13, at a given mass fraction and temperature, the solubility of CO_2 in the solutions gradually rises by increasing the partial pressure. This behavior can be described by Henry's law, in which the solubility of a gas in the aqueous solution is directly proportional to the partial pressure of the gas above the solution [74,75]. At higher partial pressure, the number of collisions between CO_2 molecules and the surface of the K-CYS solution intensified, resulting in more gas penetration into the solution and thus increasing CO_2 diffusion [16,76]. Consequently, more CO_2 molecules were absorbed into the solvent. This observation was also consistent with the finding reported by Syalsabila et al. [77], whereby, for any concentration and mass fraction, the CO_2 loading in potassium AAS of L-histidine increases at ascending pressure from 1.5 bar to 40 bar.

Table 13. CO_2 loading of K-CYS, α (mol of CO_2/mol of K-CYS), at different pressures, temperatures, and mass fraction.

10 wt.% Aqueous K-CYS					
T = 303.15 K		T = 313.15 K		T = 333.15 K	
P_{CO_2}/bar (g)	α	P_{CO_2}/bar (g)	α	P_{CO_2}/bar (g)	α
1.73	1.2864	1.79	1.2156	1.86	1.1186
4.63	1.6541	4.68	1.5565	4.69	1.4547
9.30	2.0236	9.32	1.8793	9.39	1.6955
18.05	2.5438	17.10	2.4190	17.39	2.2224
20 wt.% aqueous K-CYS					
T = 303.15 K		T = 313.15 K		T = 333.15 K	
P_{CO_2}/bar (g)	α	P_{CO_2}/bar (g)	α	P_{CO_2}/bar (g)	α
1.54	0.8425	1.78	0.7557	1.90	0.6880
4.06	1.1230	3.84	0.9677	3.99	0.8741
7.80	1.3827	8.00	1.2714	8.03	1.1572
17.90	1.9119	17.18	1.7696	17.88	1.6906

Table 13. *Cont.*

30 wt.% aqueous K-CYS					
T = 303.15 K		T = 313.15 K		T = 333.15 K	
P_{CO_2}/bar (g)	α	P_{CO_2}/bar (g)	α	P_{CO_2}/bar (g)	α
1.60	0.5259	1.96	0.4507	2.19	0.3925
3.40	0.7129	3.63	0.6516	3.98	0.5576
8.20	0.9265	8.44	0.8455	8.48	0.7109
18.00	1.2488	18.21	1.1802	17.96	1.0551

4.3.2. Effect of Temperature

In addition, Table 13 also demonstrates the effect of varying temperatures from 303.15 K to 333.15 K towards the CO_2 solubility in the aqueous K-CYS solution. Referring to Table 13, at any pressure or concentration, the solubility of CO_2 in the K-CYS solution decreases with the temperature increment, which is consistent with the Le Chatelier Principle [17,42,78]. The decrement in the CO_2 solubility is affected by the thermodynamics of the exothermic CO_2 absorption in the aqueous solution, which favors the reversible reaction at high temperatures [24]. Hence, the extent of the chemical absorption reaction was suppressed and subsequently reduced the CO_2 solubility [79,80]. Moreover, the present findings were also consistent with the trend reported by Mohsin et al. [16], whereby the CO_2 loading of glycine- 3-dimethylaminopropylamine (GLY-DMAPA) decreases as the temperature elevated from 303.15 K to 323.15 K. The authors suggested that the solvent molecules also tended to move faster due to the increased kinetic energy at higher temperatures. This phenomenon led to the breakage of intermolecular bonding, which enabled CO_2 gas to escape from the solution.

4.3.3. Effect of Solvent Concentration

At the same partial pressure of CO_2 and temperature, the concentration of solvent also poses a significant influence on CO_2 solubility. It can be seen from Figure 10 that, at constant pressure and temperature, the CO_2 loading per mol of aqueous K-CYS solution decreases with increasing solvent concentration in the order of 30 wt.% < 20 wt.% < 10 wt.%. This behavior can be attributed to the increasing number of K-CYS molecules in the solution at higher concentrations, which restricted the movement of CO_2 molecules and impeded the diffusion of CO_2 [18,52]. In another work, Aftab et al. [42] reported the reduction of CO_2 solubility in Na-βala solution from 1.651 to 1.117 mol of CO_2/mol of solvent at the same P_{CO2} and temperature, as the concentration increased from 10 wt.% to 30 wt.%. A similar trend was also observed for other types of amino acid by Mohsin et al. [16], whereby the CO_2 solubility in a 3-dimethylaminopropylamine (DMAPA)-glycine (GLY) mixture decreased as the solvent concentration increased. The author suggested that the increment of solvent concentration led to higher solutes present in the solution, suppressing CO_2 diffusion.
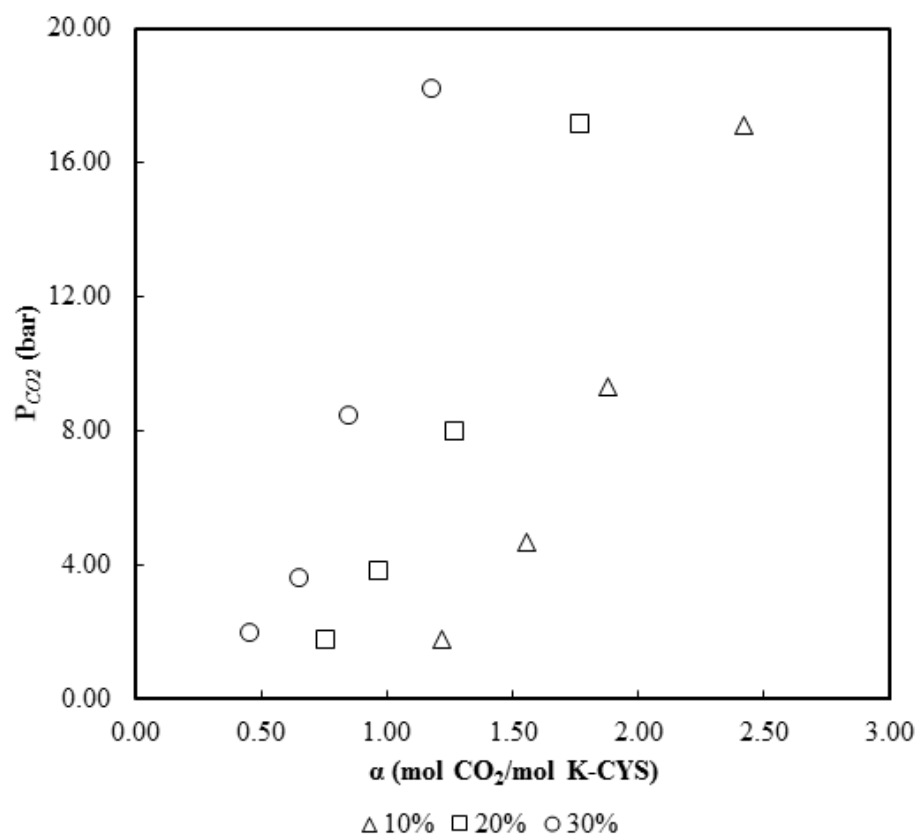
Figure 10. Effect of concentration on the solubility of CO_2 in K-CYS solutions at 313.15 K.

4.3.4. Comparison with Other Amino Acid Salt Solvents and MDEA

As shown in Figure 11, aqueous K-CYS demonstrates a higher CO_2 absorption capacity compared to other amino acid salts (AASs) such as sodium salts of β-alanines. The promising performance of K-CYS could be attributed to the more unstable carbamates formed during the reaction with CO_2, which subsequently hydrolyzed and liberated more free amine ions for CO_2 absorption. Nevertheless, the performance of K-CYS is still slightly lower compared to the potassium salts of L-phenylalanine (K-Phe) [54] and MDEA [79]. In comparison to MDEA, aqueous K-CYS has a higher molecular weight than its counterpart, which resulted in a lower number of solvent molecules present in the solvent that were available for CO_2 diffusion [31]. Therefore, this phenomenon explained the lower CO_2 loading in the K-CYS compared to MDEA. Based on the comparison between the three AASs, K-Phe exhibits the highest CO_2 absorption capacity due to its large steric hindrance compared to β-alanines and K-CYS. This attribute is rendered to the bulkier substituent group attached to the amino acid structure of K-Phe. According to Zhao et al., [81], the steric hindrance effect lowers the tendency to form stable carbamates, thus promoting CO_2 loading. Hence, this finding explained the greater equilibrium CO_2 loading demonstrated by K-Phe compared to K-CYS and β-alanines. Therefore, further research is necessary to enhance the CO_2 reactivity of K-CYS.
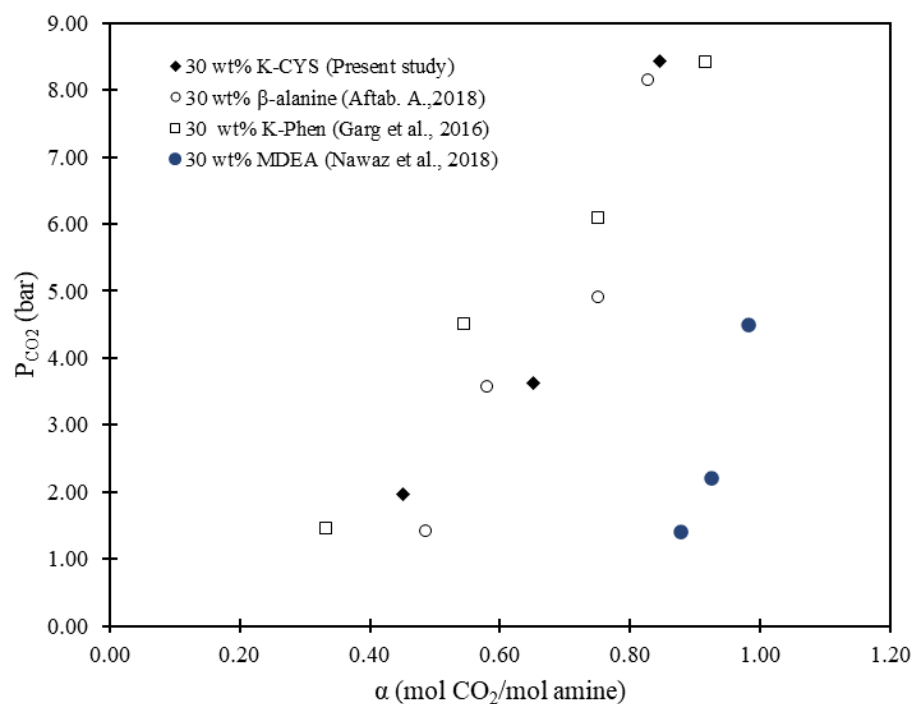
Figure 11. Comparison of experimental solubility of CO_2 in 30 wt.% K-CYS with literature data [42,54] at 313.15 K.

5. Conclusions

In this study, the capability of the potassium salt of L-cysteine (K-CYS) was investigated as a potential green solvent for CO_2 removal from natural gas. Herein, the density, viscosity, and refractive index of K-CYS solution were measured over a range of temperatures from 298.15 to 333.15 K using different mass fractions, varied from 5 to 30 wt.%. The physicochemical properties of K-CYS were observed to decrease at elevated temperatures and increase at higher mass fractions. The experimental results for all properties were also correlated as a function of temperature. The parity plot showed a good agreement between experimental and predicted data with SD $\leq$ 0.1. Hence, the empirical expressions applied can be effectively used to predict the physicochemical properties of aqueous K-CYS at other process conditions. Moreover, the present work also evaluated the thermal expansion coefficient and activation energy for K-CYS at different concentrations and temperatures based on their experimental density and viscosity. The thermal coefficient of K-CYS was found to increase linearly with the rise in temperature and solvent concentration. Meanwhile, the increment in the concentration of the solution showed a positive effect on the viscosity activation energy of K-CYS. On the other hand, the performance of aqueous K-CYS for CO_2 absorption was investigated using different solvent concentrations of 10 wt.%, 20 wt.%, and 30 wt.% under varying pressures, from 2 to 20 bar (g) and temperatures of 303.15 to 333.15 K. Based on the experiment, K-CYS demonstrated a substantially high CO_2 absorption capacity with a maximum CO_2 loading of 2.5438 mol of CO_2/mol of K-CYS attained at an equilibrium partial pressure of 18.05 bar (g). The presence of the sterically hindered amino group in K-CYS exhibited more hydroxyl ions to dissociate and bicarbonate formation during CO_2 absorption, which accounted for high CO_2 loading. The high solubility of CO_2 in K-CYS may contribute to a significant operational cost-saving in CO_2 sequestration. Therefore, by exploiting the advantages of high CO_2 absorption capacity, along with their favorable intrinsic properties such as low volatility, environmental friendliness, and resistance towards oxidative degradation, K-CYS offers a promising potential as an alternative solvent for CO_2 removal. Nevertheless, further research is necessary to enhance the reactivity and competitiveness of K-CYS on par with the industrial solvent such as MDEA for practical implementation in natural gas applications. Overall, the findings from

this study contributed a remarkable insight into the potential application of amino acid salts as a green solvent for CO_2 removal from natural gas.

References

1. International Energy Agency Southeast Asia Energy Outlook 2022. In *Southeast Asia Energy Outlook 2022*; International Energy Agency: Paris, France, 2022.
2. MacKenzie, W. *Malaysia LNG Long-Term Outlook H1 2020*; Wood MacKenzie: Edinburgh, UK, 2020.
3. Ghi, T.; Mulyo, P. Unlocking High CO_2 Gas Fields–Contributing to the Carbon Economy. 2021. Available online: https://www.adlittle.com/my-en/insights/viewpoints/unlocking-high-co2-gas-fields----contributing-carbon-economy (accessed on 26 October 2022).
4. Battersby, A. 23 Tcf of Gas Resources Require CCS in Malaysia. Available online: https://www.upstreamonline.com/energy-transition/23-tcf-of-gas-resources-require-ccs-in-malaysia/2-1-1198312 (accessed on 28 October 2022).
5. Battersby, A. "Critical Enabler": Malaysia Has Lofty Carbon Capture and Storage Ambitions. Available online: https://www.upstreamonline.com/energy-transition/critical-enabler-malaysia-has-lofty-carbon-capture-and-storage-ambitions/2-1-1198266 (accessed on 27 October 2022).
6. Isa, F.; Zabiri, H.; Singh, S.K.M.; Shariff, A.M. Dynamic Modelling for High Pressure CO_2 Absorption from Natural Gas. *Commun. Comput. Inf. Sci.* **2017**, *752*, 261–271. [CrossRef]
7. Yoo, Y.; Lee, D.; Park, J. Characteristics and Configurations of Task-Specific Deep Eutectic Solvents with CO_2-Philic Functional Groups. *J. Environ. Chem. Eng.* **2022**, *10*, 108034. [CrossRef]
8. Ye, Y.; Zhao, X.; Chen, J.; Fang, M. Pilot-Scale Experimental Study of a New High-Loading Absorbent for Capturing CO_2 from Flue Gas. *Processes* **2022**, *10*, 599. [CrossRef]
9. Mohsin, H.M.; Johari, K.; Shariff, A.M. Virgin Coconut Oil (VCO) and Potassium Glycinate (PG) Mixture as Absorbent for Carbon Dioxide Capture. *Fuel* **2018**, *232*, 454–462. [CrossRef]
10. Vega, F.; Cano, M.; Camino, S.; Fernández, L.M.G.; Portillo, E.; Navarrete, B. Solvents for Carbon Dioxide Capture. In *Capture and Oil Recovery*; Karamé, I., Shaya, J., Srou, H., Eds.; IntechOpen: Rijeka, Croatia, 2018; Chapter 8; ISBN 978-1-78923-575-3.
11. Bottoms, R.R. Process for Separating Acidic Gases. U.S. Patent US1783901, 22 December 1936.
12. Tiwari, S.C.; Bhardwaj, A.; Nigam, K.D.P.; Pant, K.K.; Upadhyayula, S. A Strategy of Development and Selection of Absorbent for Efficient CO_2 Capture: An Overview of Properties and Performance. *Process Saf. Environ. Prot.* **2022**, *163*, 244–273. [CrossRef]
13. Yu, B.; Yu, H.; Li, K.; Yang, Q.; Zhang, R.; Li, L.; Chen, Z. Characterisation and Kinetic Study of Carbon Dioxide Absorption by an Aqueous Diamine Solution. *Appl. Energy* **2017**, *208*, 1308–1317. [CrossRef]
14. Borhani, T.N.; Wang, M. Role of Solvents in CO_2 Capture Processes: The Review of Selection and Design Methods. *Renew. Sustain. Energy Rev.* **2019**, *114*, 109299. [CrossRef]

15. Font-Palma, C.; Cann, D.; Udemu, C. Review of Cryogenic Carbon Capture Innovations and Their Potential Applications. *C* **2021**, *7*, 58. [CrossRef]

16. Mohamed Mohsin, H.; Mohd Shariff, A.; Johari, K. 3-Dimethylaminopropylamine (DMAPA) Mixed with Glycine (GLY) as an Absorbent for Carbon Dioxide Capture and Subsequent Utilization. *Sep. Purif. Technol.* **2019**, *222*, 297–308. [CrossRef]

17. Wang, N.; Peng, Z.; Gao, H.; Sema, T.; Shi, J.; Liang, Z. New Insight and Evaluation of Secondary Amine/N-Butanol Biphasic Solutions for CO_2 Capture: Equilibrium Solubility, Phase Separation Behavior, Absorption Rate, Desorption Rate, Energy Consumption and Ion Species. *Chem. Eng. J.* **2022**, *431*, 133912. [CrossRef]

18. Mohsin, H.M.; Johari, K.; Shariff, A.M. Physicochemical Properties of Aqueous 2-Aminoethanoic Acid and N, N-Dimethyl-1,3-Diaminopropane as an Absorbent for Carbon Dioxide Capture. *J. Chem. Eng. Data* **2020**, *65*, 2603–2610. [CrossRef]

19. Mikulčić, H.; Skov, I.R.; Dominković, D.F.; Wan Alwi, S.R.; Manan, Z.A.; Tan, R.; Duić, N.; Hidayah Mohamad, S.N.; Wang, X. Flexible Carbon Capture and Utilization Technologies in Future Energy Systems and the Utilization Pathways of Captured CO_2. *Renew. Sustain. Energy Rev.* **2019**, *114*, 109338. [CrossRef]

20. Yoro, K.O.; Daramola, M.O.; Sekoai, P.T.; Armah, E.K.; Wilson, U.N. Advances and Emerging Techniques for Energy Recovery during Absorptive CO_2 Capture: A Review of Process and Non-Process Integration-Based Strategies. *Renew. Sustain. Energy Rev.* **2021**, *147*, 111241. [CrossRef]

21. Khalifa, O.; Alkhatib, I.I.I.; Bahamon, D.; Alhajaj, A.; Abu-Zahra, M.R.M.; Vega, L.F. Modifying Absorption Process Configurations to Improve Their Performance for Post-Combustion CO_2 Capture–What Have We Learned and What Is Still Missing? *Chem. Eng. J.* **2022**, *430*, 133096. [CrossRef]

22. Rajiman, V.; Halim, H.N.A.; Shariff, A.M.; Shahid, M.Z.; Maulud, A.S.; Lau, K.K.; Tan, L.S. CO_2 Absorption from Biogas Using Piperazine-Promoted 2-Amino-2-Methyl-1-Propanol: Process Performance in a Packed Column. *Sustainability* **2022**, *14*, 7095. [CrossRef]

23. Guo, L.; Wang, Y.; Wang, B.; Wang, N.; Zhang, L.; Chen, Y. A Simplified Semi-Empirical Model For Modelling of CO_2 Solubilities In Aqueous MDEA and MEA Solutions. *Fluid Phase Equilib.* **2022**, *555*, 113352. [CrossRef]

24. See, T.L. Absorption of High Carbon Dioxide (CO_2) Content Natural Gas In Packed Column At Elevated Pressure Using Aqeous and Hybrid Solvent. Ph.D. Thesis, Universiti Teknologi PETRONAS, Seri Iskandar, Malaysia, 2015.

25. Khan, S.N.; Hailegiorgis, S.M.; Man, Z.; Shariff, A.M. High Pressure Solubility of Carbon Dioxide (CO_2) in Aqueous Solution of Piperazine (PZ) Activated N-Methyldiethanolamine (MDEA) Solvent for CO_2 Capture. *AIP Conf. Proc.* **2017**, *1891*, 020081. [CrossRef]

26. Farooqi, A.S.; Ramli, R.M.; Lock, S.S.M.; Hussein, N.; Shahid, M.Z.; Farooqi, A.S. Simulation of Natural Gas Treatment for Acid Gas Removal Using the Ternary Blend of MDEA, AEEA, and NMP. *Sustainability* **2022**, *14*, 10815. [CrossRef]

27. Hasan, S.; Abbas, A.J.; Nasr, G.G. Improving the Carbon Capture Efficiency for Gas Power Plants through Amine-based Absorbents. *Sustainability* **2021**, *13*, 72. [CrossRef]

28. Yuan, X.; Chen, X.; Xing, J.; Fang, J.; Jin, X.; Zhang, W. Enhanced Research of Absorption by Mass Transfer Promoters. *Sep. Purif. Technol.* **2020**, *253*, 117465. [CrossRef]

29. Balchandani, S.C.; Mandal, B.; Dharaskar, S. Enrichment in CO_2 Absorption by 2-Methyl Piperazine-Activated Tertiary Amines, Physical Solvents, and Ionic Liquid Systems. *ACS Omega* **2022**, *7*, 23611–23623. [CrossRef] [PubMed]

30. Jaafari, L.; Jaffary, B.; Idem, R. Screening Study for Selecting New Activators for Activating MDEA for Natural Gas Sweetening. *Sep. Purif. Technol.* **2018**, *199*, 320–330. [CrossRef]

31. Ramezani, R.; Mazinani, S.; Di Felice, R. Density, Viscosity, PH, Heat of Absorption, and CO_2 Loading Capacity of Methyldiethanolamine and Potassium Lysinate Blend Solutions. *J. Chem. Eng. Data* **2021**, *66*, 1611–1629. [CrossRef]

32. Bao, Z.; Li, Q.; Akhmedov, N.G.; Li, B.A.; Xing, M.; Wang, J.; Morsi, B.I.; Li, B. Innovative Cycling Reaction Mechanisms of CO_2 Absorption in Amino Acid Salt Solvents. *Chem. Eng. J. Adv.* **2022**, *10*, 100250. [CrossRef]

33. Garg, S.; Shariff, A.M.; Shaikh, M.S.; Lal, B.; Aftab, A.; Faiqa, N. Surface Tension and Derived Surface Thermodynamic Properties of Aqueous Sodium Salt of L-Phenylalanine. *Indian J. Sci. Technol.* **2016**, *9*, 1–11. [CrossRef]

34. Ciftja, A.F.; Hartono, A.; Svendsen, H.F. Selection of Amine Amino Acids Salt Systems for CO_2 Capture. *Energy Procedia* **2013**, *37*, 1597–1604. [CrossRef]

35. Peu, S.D.; Das, A.; Hossain, M.S.; Akanda, M.A.M.; Akanda, M.M.H.; Rahman, M.; Miah, M.N.; Das, B.K.; Islam, A.R.M.T.; Salah, M.M. A Comprehensive Review on Recent Advancements in Absorption-Based Post Combustion Carbon Capture Technologies to Obtain a Sustainable Energy Sector with Clean Environment. *Sustainability* **2023**, *15*, 5827. [CrossRef]

36. Majchrowicz, M.E.; Brilman, D.W.F.; Groeneveld, M.J. Precipitation Regime for Selected Amino Acid Salts for CO_2 Capture from Flue Gases. *Energy Procedia* **2009**, *1*, 979–984. [CrossRef]

37. Hamzehie, M.E.; Najibi, H. Carbon Dioxide Absorption in Aqueous Solution of Potassium Glycinate + 2-Amino-2-Methyl-1-Propanol as New Absorbents. *RSC Adv.* **2016**, *6*, 62612–62623. [CrossRef]

38. Dashti, A.; Amirkgani, F.; Hamedi, A.-S.; Mohammadi, A.H. Evaluation of CO_2 Absorption by Amino Acid Salt Aqueous Solution Using Hybrid Soft Computing Methods. *ACS Omega* **2021**, *6*, 12459–12469. [CrossRef]

39. Ramezani, R.; Mazinani, S.; Felice, R. Di State-of-the-Art of CO_2 Capture with Amino Acid Salt Solutions. *Rev. Chem. Eng.* **2020**, *38*, 273–299. [CrossRef]

40. Hu, G.; Smith, K.H.; Wu, Y.; Mumford, K.A.; Kentish, S.E.; Stevens, G.W. Carbon Dioxide Capture by Solvent Absorption Using Amino Acids: A Review. *Chin. J. Chem. Eng.* **2018**, *26*, 2229–2237. [CrossRef]

41. Song, H.-J.; Park, S.; Kim, H.; Gaur, A.; Park, J.-W.; Lee, S.-J. Carbon Dioxide Absorption Characteristics of Aqueous Amino Acid Salt Solutions. *Int. J. Greenh. Gas Control* **2012**, *11*, 64–72. [CrossRef]
42. Aftab, A.; Shariff, A.M.; Garg, S.; Lal, B.; Shaikh, M.S.; Faiqa, N. Solubility of CO_2 in Aqueous Sodium β-Alaninate: Experimental Study and Modeling Using Kent Eisenberg Model. *Chem. Eng. Res. Des.* **2018**, *131*, 385–392. [CrossRef]
43. Chang, Y.-T.; Leron, R.B.; Li, M.-H. Carbon Dioxide Solubility in Aqueous Potassium Salt Solutions of L-Proline and Dl-α-Aminobutyric Acid at High Pressures. *J. Chem. Thermodyn.* **2015**, *83*, 110–116. [CrossRef]
44. Sartori, G.; Savage, D.W. Sterically Hindered Amines for CO_2 Removal from Gases. *Ind. Eng. Chem. Fundam.* **1983**, *22*, 239–249. [CrossRef]
45. Balchandani, S.; Mandal, B.; Garg, S.; Li, M.; Dharaskar, S. Physicochemical and Thermodynamic Properties of Aqueous Blends of 3-Aminopropyl Triethoxysilane and Amines at 298.15–333.15 K. *J. Mol. Liq.* **2021**, *332*, 115440. [CrossRef]
46. Murshid, G.; Ghaedi, H.; Ayoub, M.; Garg, S.; Ahmad, W. Experimental and Correlation of Viscosity and Refractive Index of Non-Aqueous System of Diethanolamine (DEA) and Dimethylformamide (DMF) for CO_2 Capture. *J. Mol. Liq.* **2018**, *250*, 162–170. [CrossRef]
47. Murshid, G.; Ali, A.; Garg, S.; Al-jabri, S.; Mubashir, M.; Loke, P. Model Analysis for Development of Piperazine Activated Sodium Sarcosinate Solutions for Environmental Sustainability. *Sustain. Energy Technol. Assess.* **2022**, *53*, 102509. [CrossRef]
48. Shaikh, M.S.; Shariff, A.M.; Bustam, M.A.; Murshid, G. Physical Properties of Aqueous Solutions of Potassium Carbonate + glycine as a Solvent for Carbon Dioxide Removal. *J. Serb. Chem. Soc.* **2014**, *79*, 719–727. [CrossRef]
49. Ab Rahim, A.H.; Yunus, N.M.; Jaffar, Z.; Allim, M.F.; Othman Zailani, N.Z.; Mohd Fariddudin, S.A.; Abd Ghani, N.; Umar, M. Synthesis and Characterization of Ammonium-Based Protic Ionic Liquids for Carbon Dioxide Absorption. *RSC Adv.* **2023**, *13*, 14268–14280. [CrossRef] [PubMed]
50. He, F.; Wang, T.; Fang, M.; Wang, Z.; Yu, H.; Ma, Q. Screening Test of Amino Acid Salts for CO_2 Absorption at Flue Gas Temperature in a Membrane Contactor. *Energy Fuels* **2017**, *31*, 770–777. [CrossRef]
51. Aftab, A. Physical Properties and CO_2 Solubility of Aqueous Sodium and Potassium Salts of β-Alanine. Master's Thesis, Universiti Teknologi PETRONAS, Seri Iskandar, Malaysia, 2018.
52. Zarei, A.; Hafizi, A.; Rahimpour, M.R.; Raeissi, S. Carbon Dioxide Absorption into Aqueous Potassium Salt Solutions of Glutamine Amino Acid. *J. Mol. Liq.* **2020**, *301*, 111743. [CrossRef]
53. Murshid, G.; Ahmad Butt, W.; Garg, S. Investigation of Thermophysical Properties for Aqueous Blends of Sarcosine with 1-(2-Aminoethyl) Piperazine and Diethylenetriamine as Solvents for CO_2 Absorption. *J. Mol. Liq.* **2019**, *278*, 584–591. [CrossRef]
54. Garg, S.; Shariff, A.M.; Shaikh, M.S.; Lal, B.; Aftab, A.; Faiqa, N. VLE of CO_2 in Aqueous Potassium Salt of L-Phenylalanine: Experimental Data and Modeling Using Modified Kent-Eisenberg Model. *J. Nat. Gas Sci. Eng.* **2016**, *34*, 864–872. [CrossRef]
55. Harris, F. A Study on the Potential of Amino Acid Salt as a Solvent for Acid Gas Removal. Master's Thesis, Universiti Teknologi PETRONAS, Seri Iskandar, Malaysia, 2009.
56. Khodadadi, M.J.; Riahi, S.; Abbasi, M. Experimental Modeling of the Solubility of Carbon Dioxide in Aqueous Solution of Monoethanolamine +1, 3-Diaminopropane. *J. Mol. Liq.* **2019**, *281*, 415–422. [CrossRef]
57. Bohloul, M.R.; Vatani, A.; Peyghambarzadeh, S.M. Experimental and Theoretical Study of CO_2 Solubility in N-Methyl-2-Pyrrolidone (NMP). *Fluid Phase Equilib.* **2014**, *365*, 106–111. [CrossRef]
58. National Center for Biotechnology Information PubChem Compound Summary for CID 5862, Cysteine. Available online: https://pubchem.ncbi.nlm.nih.gov/compound/Cysteine (accessed on 25 September 2022).
59. Podolsky, N.E.; Marcos, M.A.; Cabaleiro, D.; Semenov, K.N.; Lugo, L.; Petrov, A.V.; Charykov, N.A.; Sharoyko, V.V.; Vlasov, T.D.; Murin, I.V. Physico-Chemical Properties of C 60 (OH) 22–24 Water Solutions: Density, Viscosity, Refraction Index, Isobaric Heat Capacity and Antioxidant Activity. *J. Mol. Liq.* **2019**, *278*, 342–355. [CrossRef]
60. Garg, S.; Murshid, G.; Mjalli, F.S.; Ali, A.; Ahmad, W. Experimental and Correlation Study of Selected Physical Properties of Aqueous Blends of Potassium Sarcosinate and 2-Piperidineethanol as a Solvent for CO_2 Capture. *Chem. Eng. Res. Des.* **2017**, *118*, 121–130. [CrossRef]
61. Gao, H.; Gao, G.; Liu, H.; Luo, X.; Liang, Z.; Idem, R.O. Density, Viscosity, and Refractive Index of Aqueous CO_2-Loaded and -Unloaded Ethylaminoethanol (EAE) Solutions from 293.15 to 323.15 K for Post Combustion CO_2 Capture. *J. Chem. Eng. Data* **2017**, *62*, 4205–4214. [CrossRef]
62. Ullah, S.; Azmi Bustam, M.; Sagir, M.; Ali Assiri, M.; Al-Sehemi, A.G.; Ayoub, M.; Inayat, A.; Mukhtar, A.; Saqib, S.; Babar, M.; et al. CO_2 Solubility and Thermophysical Properties in Aqueous Mixtures of Piperazine and Diethanolamine. *Sustain. Energy Technol. Assess.* **2022**, *53*, 102514. [CrossRef]
63. Pandey, D.; Mondal, M.K. Viscosity, Density, and Derived Thermodynamic Properties of Aqueous 2-(Ethylamino)Ethanol (EAE), Aqueous Aminoethylethanolamine (AEEA), and Its Mixture for Post-Combustion CO_2 Capture. *J. Mol. Liq.* **2021**, *332*, 115873. [CrossRef]
64. Li, H.; Guo, H.; Shen, S. Water-Lean Blend Mixtures of Amino Acid Salts and 2-Methoxyethanol for CO_2 Capture: Density, Viscosity and Solubility of CO_2. *J. Chem. Thermodyn.* **2020**, *150*, 26–28. [CrossRef]
65. Khan, S.N.; Hailegiorgis, S.M.; Man, Z.; Shariff, A.M.; Garg, S. Thermophysical Properties of Aqueous 1-Butyl-3-Methylimidazolium Acetate [BMIM] [AC] + Monoethanolamine (MEA) Hybrid as a Solvent for CO_2 Capture. *Procedia Eng.* **2016**, *148*, 1326–1331. [CrossRef]

66. Guo, H.; Hui, L.; Shen, S. Monoethanolamine + 2-Methoxyethanol Mixtures for CO_2 Capture: Density, Viscosity and CO_2 Solubility. *J. Chem. Thermodyn.* **2019**, *132*, 155–163. [CrossRef]

67. Garg, S.; Shariff, A.M.; Shaikh, M.S.; Lal, B.; Aftab, A.; Faiqa, N. Selected Physical Properties of Aqueous Potassium Salt of L-Phenylalanine as a Solvent for CO_2 Capture. *Chem. Eng. Res. Des.* **2016**, *113*, 169–181. [CrossRef]

68. Tellagorla, R.; Balchandani, S.C.; Das, P.; Mandal, B.; Gumma, S. Measurement and Correlations of Physicochemical Properties of the Novel Solvent Tris(2-Aminoethyl) Amine and Its Blend with N-Methyldiethanolamine and 2-Amino 2-Methyl-1-Propanol. *J. Chem. Eng. Data* **2022**, *67*, 2067–2076. [CrossRef]

69. Aziz, N.F.A.; Shariff, A.M.; Shaikh, M.S.; Keong, L.K.; Garg, S.; Aftab, A. Physical Properties of Aqueous Sodium Salt Solution of α-Methylalanine (Na-AMALA). *Procedia Eng.* **2016**, *148*, 444–450. [CrossRef]

70. Garg, S. Physicochemical and Thermodynamic Properties of Aqueous Blends of 3-Aminopropyl Triethoxysilane and Amines at 298.15–333.15 K. Master's Thesis, Universiti Teknologi PETRONAS, Seri Iskandar, Malaysia, 2016.

71. Zhang, P.; Ji, Y.; Li, W.; Xu, L.; Wang, L.; Fu, D. Investigation of Viscosity, Activation Energy and CO_2 Diffusion Coefficient for N-Methyl-1,3-Propane-Diamine, N-(2-Aminoethyl)Ethanolamine and 1,4-Butanediamine Activated 2-Diethylaminoethanol Aqueous Solutions. *J. Chem. Thermodyn.* **2022**, *168*, 106740. [CrossRef]

72. Perumal, M.; Jayaraman, D.; Balraj, A. Experimental Studies on CO_2 Absorption and Solvent Recovery in Aqueous Blends of Monoethanolamine and Tetrabutylammonium Hydroxide. *Chemosphere* **2021**, *276*, 130159. [CrossRef]

73. Shen, K.; Li, M.-H. Solubility of Carbon Dioxide in Aqueous Mixtures of Monoethanolamine and Methyldiethanolamine. *J. Chem. Eng. Data* **1992**, *37*, 96–100. [CrossRef]

74. Li, L.; Burns, R.C.; Maeder, M.; Puxty, G.; Wang, S.; Yu, H. The Determination of the Henry's Coefficient of Reactive Gases–An Example of CO_2 in Aqueous Solutions of Monoethanolamine (MEA). *Chem. Eng. Sci.* **2017**, *173*, 474–482. [CrossRef]

75. Schmitz, K.S. *Thermodynamics of the Liquid State*; Elsevier: Amsterdam, The Netherlands, 2017; ISBN 9780128005149.

76. Garg, S.; Shariff, A.M.; Shaikh, M.S.; Lal, B.; Suleman, H.; Faiqa, N. Experimental Data, Thermodynamic and Neural Network Modeling of CO_2 Solubility in Aqueous Sodium Salt of L-Phenylalanine. *Biochem. Pharmacol.* **2017**, *19*, 146–156. [CrossRef]

77. Syalsabila, A.; Maulud, A.S.; Suleman, H.; Md Nordin, N.A.H. VLE of Carbon Dioxide-Loaded Aqueous Potassium Salt of L-Histidine Solutions as a Green Solvent for Carbon Dioxide Capture: Experimental Data and Modelling. *Int. J. Chem. Eng.* **2019**, *2019*, 9428638. [CrossRef]

78. Zahari, N.A.S.M. Experimental Measurements and Thermodynamic Modeling of Carbon Dioxide Solubility in Blends of Aqueous Potassium Lysinate with Piperazine and 2-Amino-2-Methyl-1-Propanol. Master's Thesis, Universiti Teknologi PETRONAS, Seri Iskandar, Malaysia, 2019.

79. Nawaz, S.; Mekuria, S.; Man, Z.; Garg, S.; Mohd, A.; Farrukh, S.; Ayoub, M.; Ghaedi, H. High-Pressure Absorption Study of CO_2 in Aqueous N-Methyldiethanolamine (MDEA) and MDEA-Piperazine (PZ)-1-Butyl-3-Methylimidazolium Tri Fl Uoromethane-sulfonate [Bmim][OTf] Hybrid Solvents. *J. Mol. Liq.* **2018**, *249*, 1236–1244. [CrossRef]

80. Shariff, A.M.; Shaikh, M.S.; Bustam, M.A.; Garg, S.; Faiqa, N.; Aftab, A. High-Pressure Solubility of Carbon Dioxide in Aqueous Sodium L- Prolinate Solution. *Procedia Eng.* **2016**, *148*, 580–587. [CrossRef]

81. Zhao, Y.; Ho, W.S.W. Steric Hindrance Effect on Amine Demonstrated in Solid Polymer Membranes for CO_2 Transport. *J. Memb. Sci.* **2012**, *415–416*, 132–138. [CrossRef]